Direct inducer cavitation instability identification using high speed visualization

Youngkuk Yoon*, and *Seung Jin* Song†

Seoul National University, Department of Mechanical Engineering

Abstract. Direct identification of inducer cavitation instability was conducted via high speed video footage without pressure information. A two-bladed inducer undergoing alternate blade cavitation has been tested. The fluctuation of grayscale values for each pixel were shown to be closely correlated with the actual pressure fluctuation. Using each frame of the high speed video footage, not only the classic visual inspection, but also quantitative method including traveling wave energy analysis and mode analysis was performed. By only using the pixel grayscale fluctuation data, quantitative methods, which have been only applied to the pressure signals to identify the cavitation instabilities, were also successively applied and the type of cavitation instability was well determined.

1 Introduction

The inducer cavitation instabilities, which are caused by the peculiar cavitation structure at the inducer with relatively low cavitation numbers, manifest themselves as an excitation of certain frequency values of the pressure signals. Figure 1 from Tsujimoto [5] shows the typical pressure signal fluctuation when the cavitation instabilities exist at the three-bladed inducer. Briefly, for odd number bladed inducer (usually three-bladed), three types of local cavitation instabilities exist: supersynchronous rotating cavitation which shows higher frequency than the shaft rotating frequency, synchronous rotating cavitation (or also called as asymmetric cavitation), which shows the same frequency as the shaft rotating frequency, and subsynchronous rotating cavitation which shows lower frequency than the shaft rotating frequency. Also, for the even number bladed inducer (two or four bladed inducer), an additional cavitation instability called alternate blade cavitation occurs. It manifests itself as half of the blade passing frequency. From various observations including Franc [1], it was shown that these kinds of 'local' cavitation instabilities, which is in contrary with 'system' instability of

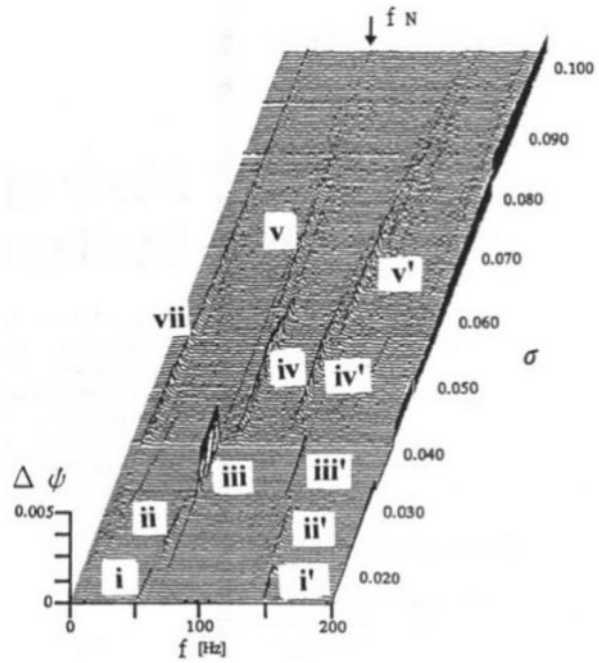

Fig. 1. Inducer cavitation instabilities for three-blade inducer

zeroth spatial harmonics such as surge, are rotating instabilities that propagate in a certain direction. To capture this rotating instabilities, unsteady pressure signal at the inducer inlet was measured to characterize those instabilities. However, because the instability is propagating, only the frequency of the instability can be known if the pressure signal was obtained from the single point. To completely know the rotating instability, its propagating direction and spatial mode (also the cell number) should be carefully determined. To determine all

* *Youngkuk* Yoon: truesky1218@snu.ac.kr
† *Seung Jin* Song: sjsong@snu.ac.kr

three components (frequency, propagating direction, and cell number) of the rotating instability, many pressure sensors should be deployed to the inducer casing. More specifically, at least 2M+1 pressure sensors are needed to determine up to Mth spatial mode (Nyquist criterion). Because of the flow interference and price issues, to determine the type of rotating instability, visualization of the cavitation instability is accompanied with two unsteady pressure sensors. While circumferentially separated two pressure sensors can identify the frequency and phase difference between two signals, we can limit the possible type of the cavitation instability. Therefore, with the aid of visual inspection, cavitation instability can be usually determined. Figure 2 shows the typical example of the inducer cavitation instability visualization.

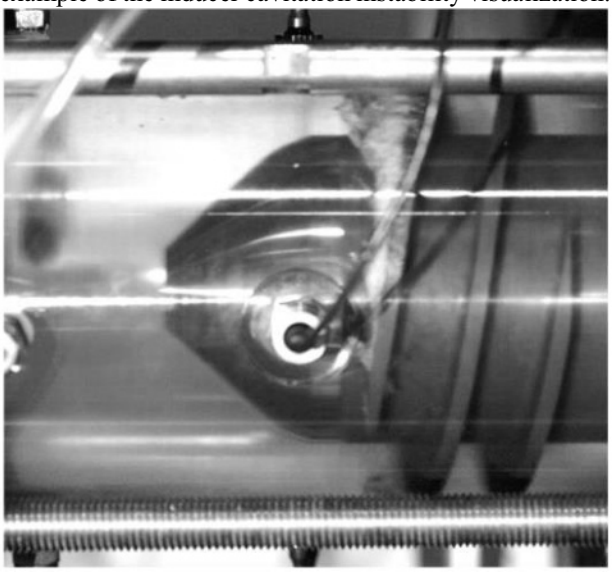

Fig. 2. Actual photo of a cavitating two-bladed inducer

However, there are certain limitations to determine the cavitation instability through intuitive visual inspections. First, the direct relation between the fluctuation of cavitation images and the actual pressure fluctuation data has to be only assumed. Also, even though the cavity is responsible for most of the pressure fluctuation in two-phase flows, the visualized cavitations might differ from the actual rotating instabilities, especially for the case of multifrequency instabilities. Therefore, for the cases where visual inspection easily fails or exact quantitative measures are needed, pertinent postprocessing of the video footages is necessary and the relation between fluctuation of image and pressure should be more closely examined. Present paper describes the direct relation between the pixel grayscale fluctuation and the pressure fluctuation signals, and, furthermore, applies various quantitative methods to the pixel grayscale fluctuation data to quantitatively determine the exact type of cavitation instability for two-bladed inducer undergoing alternate blade cavitation as a representative case.

2 Experimental setup

To obtain the clear video footage of the two-bladed inducer undergoing alternate blade cavitation, acrylic casing was used. Also, an unsteady pressure transducer (Kulite HKM-375) was flush-mounted at the inlet of the inducer, which is 0.2 diameter upstream from the inducer tip leading edge. The pressure signal from the unsteady pressure transducer was used to assure the relation between the pressure signal fluctuation and the pixel grayscale fluctuation. The video footage of the inducer was acquired using the high-speed camera (Phantom v2640) with 4800 fps, 4M pixels with bit depth of 12-bit. 1,000 successive frames were analyzed to determine the inducer cavitation instability. The overall schematic diagram for the inducer test facility is shown in Figure 3.

3 Results and discussion

Firstly, to take full advantage from the images, the correspondence between fluctuations of the image pixel grayscale and pressure signal was investigated. Figure 4 shows the amplitude of the Fourier coefficient for each pixels in the image for first to sixth harmonics of shaft rotating frequency. The brighter part denotes the stronger fluctuation of pixel grayscale values. As one might expect, while the test body is two-bladed inducer, second harmonics are excited across the entire inducer region. However, because of the inducer is undergoing the alternate blade cavitation, the amplitude of the first harmonics should be expected to show the peak value. From the figure, the amplitude of the first harmonics is highest in the cavity region and suggesting the existence of alternate blade cavitation. To investigate the correspondence between the pixel grayscale fluctuation and the pressure fluctuation, the normalized amplitude of the pixel grayscale fluctuation is compared with the actual pressure fluctuation obtained by the unsteady pressure transducer at the inducer inlet as shown in Figure 5. The shaft rotating frequency shows the highest peak in the pressure signal because of the alternate blade cavitation. Also, Figure 6 shows the pixel grayscale fluctuation which is circumferentially averaged for the better comparison and to see the contribution for the pixel grayscale fluctuation for each axial position. From the comparison between Figure 5 and 6, it is shown that the ratio between first and second harmonics shows very good agreements. Also at least up to sixth harmonics, general amplitude tendency agrees. The only discrepancy is the third harmonics, which is larger than fourth harmonics in the image analysis but smaller than the fourth harmonics in the pressure signal. To discuss this discrepancy more clearly, Figure 6 is re-drawn to Figure 7, to see the contribution of each axial position to grayscale fluctuation. As shown in Figure 7, basically three regions can be identified. First, the large amplitude is caused by the cavity fluctuation in the middle of the image, and downstream from the cavity, even number harmonics were excited by the grayscale fluctuation caused by the underlying blade passing. Lastly, upstream of the cavity region is excited due to the whirling motion of the axis (to be further announced, this is due to the uneven loading

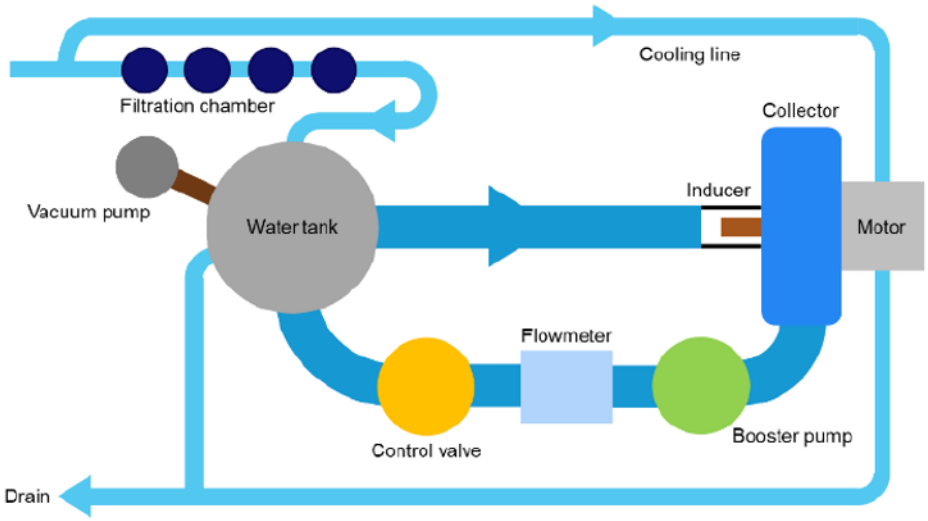

Fig. 3. Schematic diagram of the inducer test facility

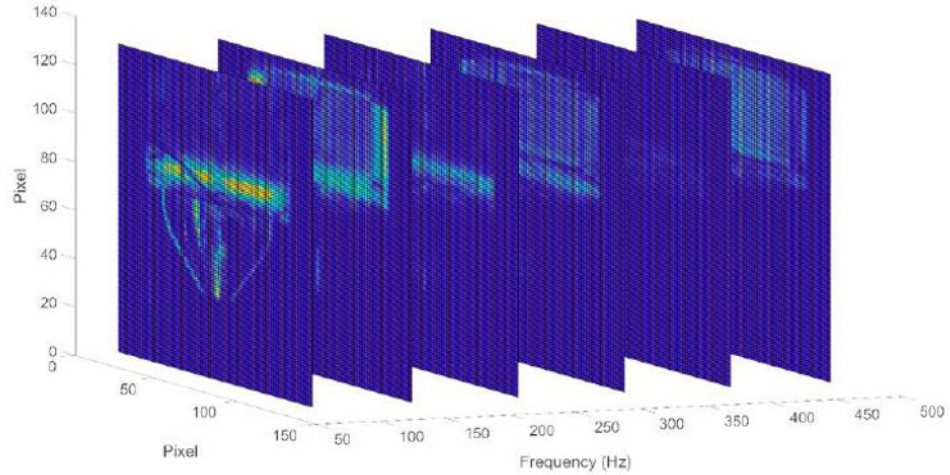

Fig. 4. Fourier coefficient amplitude of each pixel

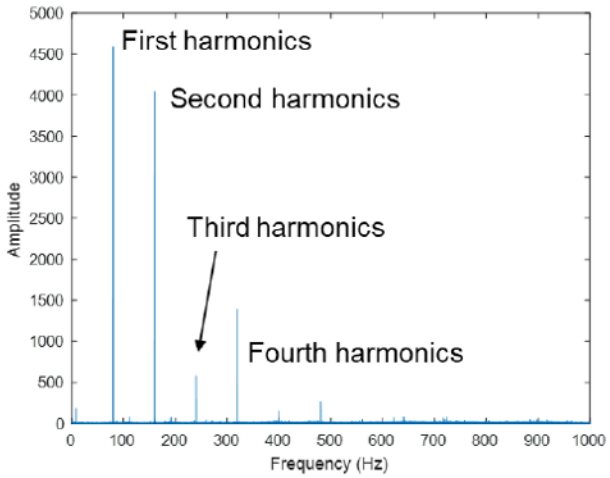

Fig. 5. FFT results of the pressure signal

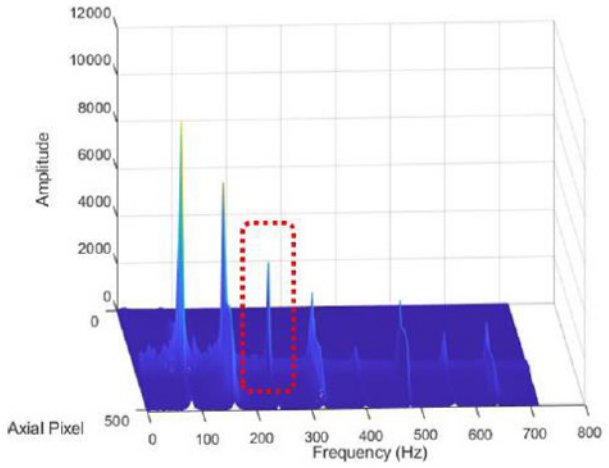

Fig. 6. Circumferentially average Fourier coefficient amplitute

to the axis caused by the alternate blade cavitation). From Figure 7, the peak axial location of the third harmonics is a little bit behind of the main cavity fluctuation region. To display it more precisely, the main cavity region and the peak axial position of third harmonics are drawn in Figure 8. The red region shows the region of pixel grayscale fluctuation due to cavity and the orange line shows the third harmonics peak position. From the video footage, the orange line is the position of tip leakage vortex cavity trailing edge. Therefore, the over-excitation of the third harmonics at the pixel grayscale fluctuation can be attributed to the fluctuation of cavity trailing edge, which is not reflected to the pressure fluctuation of the inducer inlet. This high frequency component is possibly due to the interaction of tip leakage vortex cavity with

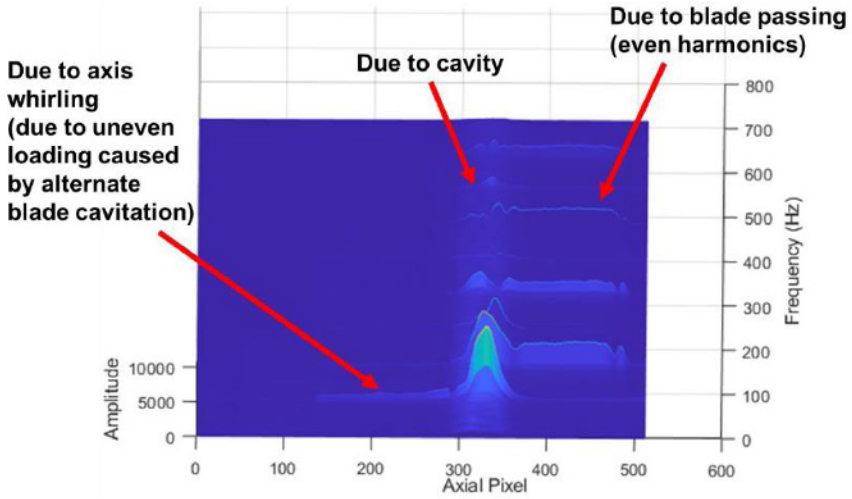

Fig. 7. Contribution of each axial position in pixel grayscale fluctuation

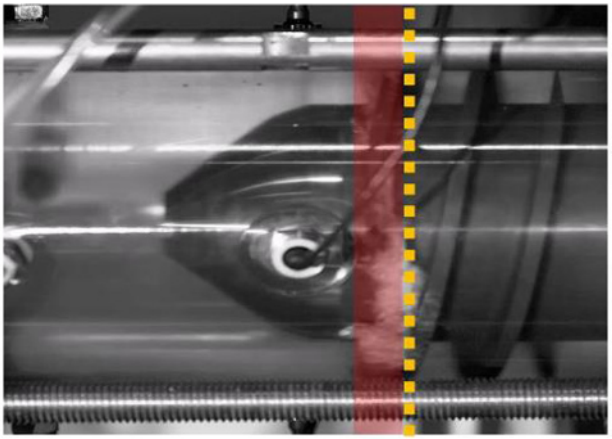

Fig. 8. Cavity region and the peak axial location for the third harmonics

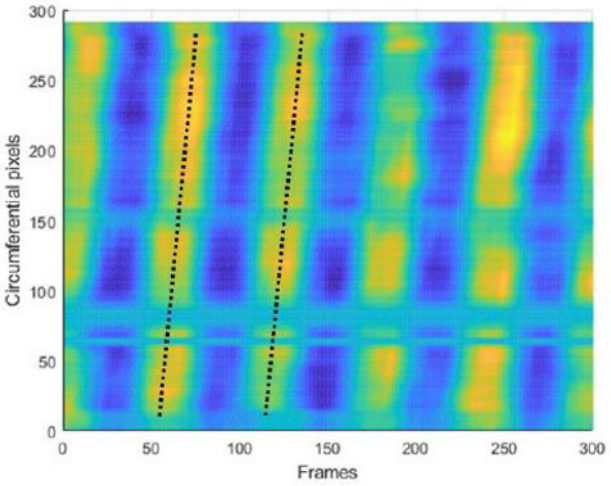

Fig. 9. Grayscale values for each circumferential pixel

the abrupt pressure gradient near adjacent blade leading edge as suggested by Liu [2]. On the other hand, the third harmonics excitation can be due to tip leakage vortex meandering caused by vortex breakdown in the vicinity of tip leakage vortex cavity trailing edge as proposed by Miorini [3]. In both cases, the over-excitation of the third harmonics can be attributed to the peculiar behavior of the tip leakage vortex cavity trailing edge and except this minor discrepancy, the ratio between other harmonics at least up to sixth harmonics showed reasonably good agreement.

Hence, the correspondence between the image grayscale fluctuation and the pressure fluctuation has been successfully shown, and, therefore, instead of using the image data as mere supplement of the pressure signal, the cavitation instabilities were identified only through visual data. To fully exploit the pixel grayscale values, firstly, time-wise evolution of all pixels in circumferential direction at representative axial position were investigated to clarify the rotating instability. Figure 9 shows the raw grayscale values for all available circumferential pixels in time-wise sequence. As shown in the figure, the bright area, which corresponds to the actual bright area in the image with high grayscale values, propagate in positive circumferential direction as time passes by and showed positive slope. Therefore, the rotating instability is clearly propagating in positive direction (or blade rotating direction). Furthermore, the spatial mode of the rotating frequency can be determined through the method shown in Figure 10. While the frequency and the propagating direction can be determined from Figure 9, the propagation trace can be drawn with assuming various spatial modes. For example, if the rotating instability has first spatial mode, the phase of the disturbances should advance about 360 degrees as the actual circumferential angle proceeds 360 degrees. For second spatial mode, the phase of the disturbances should advance 720 degrees as the actual angle

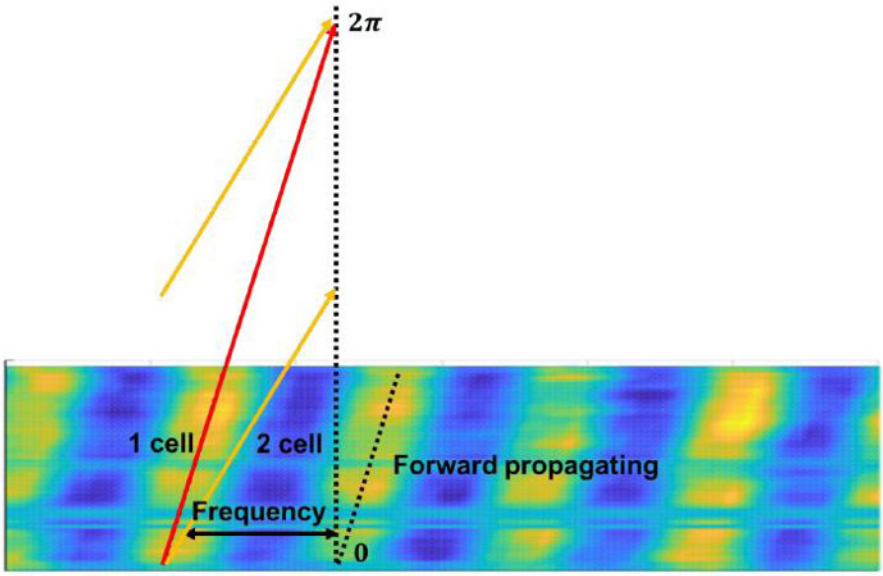

Fig. 10. Trace of the forward propagating rotating instabilities with various cell numbers

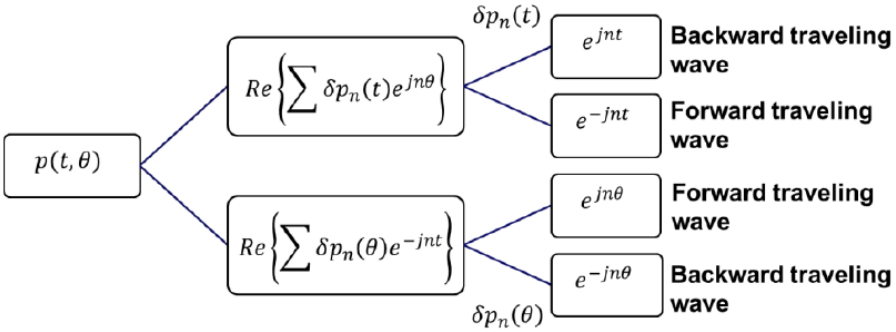

Fig. 11. Schematic diagram of the traveling wave energy analysis and mode analysis

advances 360 degrees. While we know the actual circumferential position of each pixel with geometrical relation, one can draw the traces of expected disturbances with specific spatial mode as Figure 10 and match with the figure. From the above method, the spatial mode of the rotating instability can be determined as first mode and while the instability is forward rotating, shaft rotating frequency, and first spatial mode, it can be concluded that the rotating instability is alternate blade cavitation for two-bladed inducer.

However, this trace identification cannot exclude visual inspection neither and only the most dominant rotating instability can be captured. Hence with a few selected pixels, spatial & temporal Fourier analysis were applied to quantitatively identify the rotating instability without any autonomous visual inspection. Two methods were used to test the identification capacity of the image data; traveling wave energy analysis (first suggested by Tryfonidis [4]) and mode analysis (see Figure 11). To briefly explain the application of both method, the traveling wave energy analysis first decompose the fluctuating signal into different spatial mode using spatial Fourier transform and also decompose each spatial Fourier coefficient temporally, to testify which direction of traveling wave is dominant in the certain mode. The mode analysis is quite different, that it conducts the temporal Fourier transform to the data first, to get the frequency peaks. Then, each frequency elements are decomposed into spatial modes to find which spatial mode is dominant at the certain frequency. It should be noted that while the direct relation between the grayscale value of each pixel and the pressure value is missing, only the 'normalized' fluctuation of each pixel was used. In the present paper, all the grayscale values of the image were zero-meaned and matched to have same standard variation of 100. However, this leads to the exclusion of zeroth spatial harmonics such as surge-like system instabilities. Hence, the limitation of the method is that only the local inducer cavitation

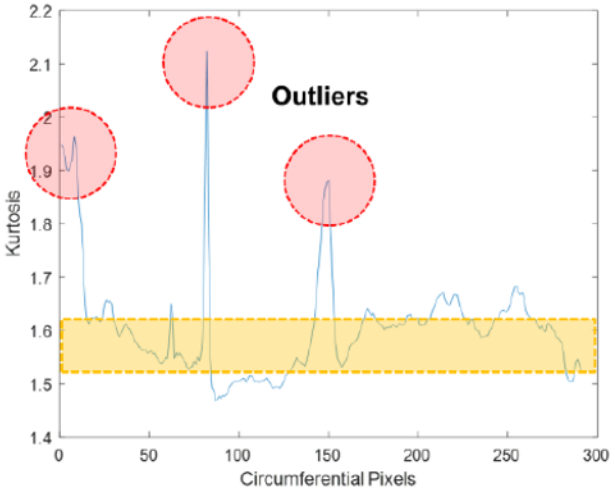

Fig. 12. Kurtosis for each circumferential pixel

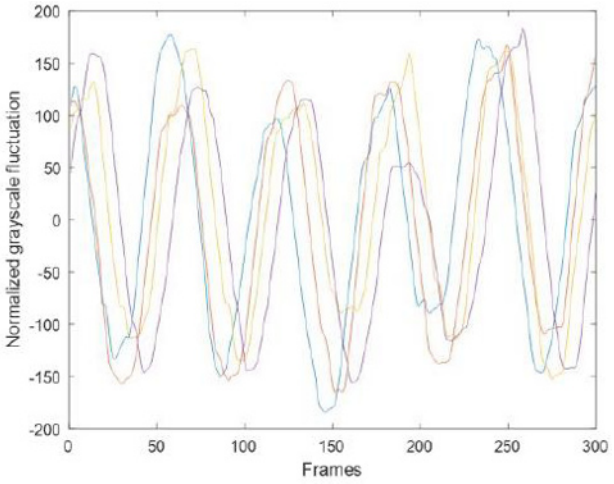

Fig. 13. Normalized grayscale values for selected pixels

instabilities can be detected through image analysis. To select the 'well-defined' pixels in circumferential direction, the kurtosis of each pixel grayscale fluctuation was investigated while the data were normalized to all have same standard deviation. Figure 12 shows kurtosis of each pixel in circumferential direction and the outliers caused by the cable in the image or other disturbance factors were clearly spotted. While selecting the pixels to conduct the above quantitative methods, those outliers were removed and equally spaced four pixels were selected while the distance between pixels were maximized to guarantee low condition number of the Fourier transformation matrix. Figure 13 shows the normalized grayscale fluctuation for selected pixels.

Figure 14 and 15 show the results of traveling wave energy analysis and the mode analysis at peak frequency of shaft rotating frequency. From Figure 14, the distinct positive peak at first harmonics for the first spatial mode was appeared and only from the visual data, we can assure that the rotating instability is forward traveling with single cell, which is again alternate blade cavitation. Also, Figure 15 re-assures that the rotating instability is the alternate blade cavitation while at the first harmonics, the positive first spatial mode is surely dominant over other modes. Hence, we can confidently assure that the instability is alternate blade cavitation.

However, the identification of the rotating instability only through side-viewed video footage has some limitations. First of all, as mentioned above, while only the fluctuating component of the pixel grayscale values was used, the system instabilities such as cavitation surge cannot be captured. Also, in case of using side-recorded video

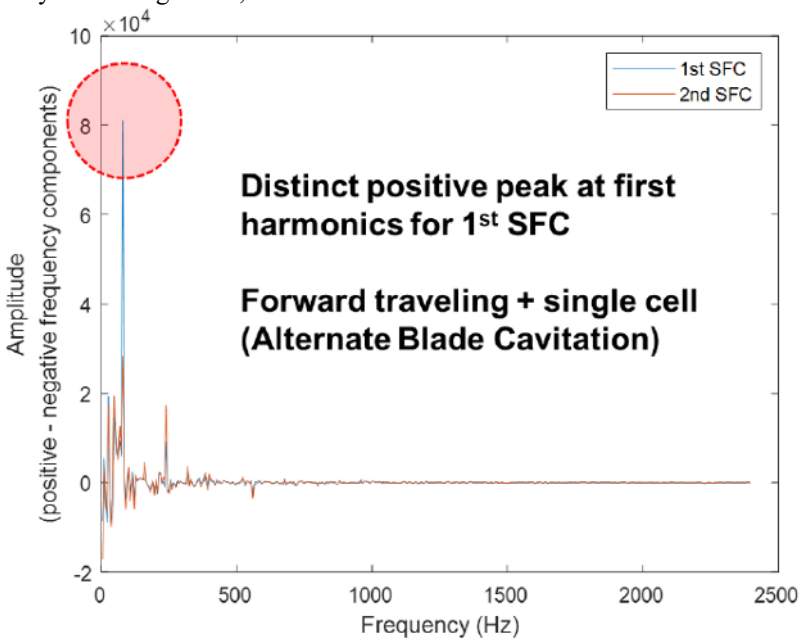

Fig. 14. Results of traveling wave energy analysis

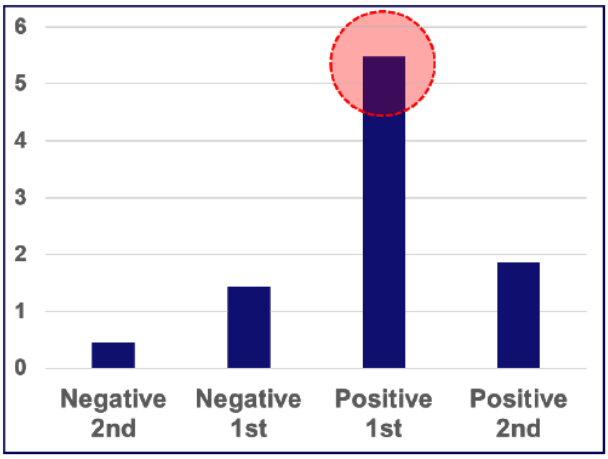

Fig. 15. Results of mode analysis

footages, because of the narrow field of view, only up to second spatial harmonics can be identified. To properly decompose the grayscale fluctuations into spatial modes, Fourier transform is conducted. Although it is theoretically possible to decompose the fluctuations into almost infinite spatial modes only via narrow window (the pixel number in circumferential direction is over 1,000), it is practically impossible with the real data to decompose it while the condition number of the Fourier transformation matrix gets exponentially larger if we try to decompose more than third spatial modes. For example, for the field of view used in present paper, the condition number for identifying up to second spatial modes is around 60, but for decomposing up to third and fourth spatial modes, the condition number is about 2,400 and 95,000. Therefore, very small noise in the data can cause the absurd results. Nevertheless, while the inducer cavitation instabilities are mainly composed by the first or second spatial mode because of the small blade number of blades, the present analysis can well capture the inducer cavitation instability directly from the video footage.

4 Concluding remarks

Without using the pressure signals, using the correspondence between the pixel grayscale values and the pressure signal fluctuations, local cavitation instabilities can be successively identified. Also, pixel information can contain the pressure fluctuation information, especially for first and second spatial modes. Furthermore, it has been shown from the present analysis that not only visual inspection, but other quantitative identification methods such as traveling wave analysis and mode analysis can be well applied to the image analysis.

5 Acknowledgments

This work was supported by the Agency for Defense Development under the basic research program.

References

1. J. -P. Franc, G. Boitel, M. Riondet, É. Janson, P. Ramina, C. Rebattet, *Thermodynamic Effect on a Cavitating Inducer—Part II: On-Board Measurements of Temperature Depression Within Leading Edge Cavities*, J. Fluids Eng., **132**(2), p. 021304 (2010)
2. Y. Liu, L. Tan, *Spatial–Temporal Evolution of Tip Leakage Vortex in a Mixed-Flow Pump With Tip Clearance*, J. Fluids Eng., **141**(8) (2019)
3. R. L. Miorini, H. Wu, J. Katz, *The internal structure of the tip leakage vortex within the rotor of an axial waterjet pump*, J. Turbomach. Trans. ASME, **134**(3), p. 031018 (2012)
4. M. Tryfonidis, O. Etchevers, J. Paduano, A. Epstein, G. Hendricks, *Pre-stall behavior of several high-speed compressors*, Proc. ASME 1994 International Gas Turbine and Aeroengine Congress and Exposition, American Society of Mechanical Engineers, pp. V001T001A135-V001T001A135.
5. Y. Tsujimoto, Y. Yoshida, Y. Maekawa, S. Watanabe, T. Hashimoto, *Observations of oscillating cavitation of an inducer*, J. Fluids Eng., **119**(4), pp. 775-781 (1997)